Chapter 2

Micromachined Hot-Wire Anemometers

2.1 Introduction

A hot-wire anemometer is a device for measurement of air flow velocity, velocity fluctuation, and sometimes flow direction. In a typical hot-wire anemometer, there is a small-diameter, temperature-sensitive, resistive metal wire which is heated by passing an electric current through it. When exposed to a gas flow, the heated wire loses heat to the flow by convection and its electrical parameters such as voltage change. The velocity of the flow is then correlated to the measurement results of those parameters. Typically, the electrical arrangements are in either a constant current (CC) mode or a constant temperature (CT) mode. The CC mode is easy to implement but the CT mode performs better and hence is widely used. The documented use of hot-wire anemometer can be traced back to more than 80 years ago [1] and numerous forms of hot-wire anemometers have been devised. Nowadays, they are simply the most popular flow instruments used for laboratory fluid mechanics study. The main reason is because of their unique advantages of being simple, small, highly sensitive and relatively inexpensive.

Figure 2.1 shows an example of today's typical hot-wire anemometers used for wind-tunnel flow measurements. A metal wire is welded or soldered to two metal needles that are molded to a probe body. The wire is often made of platinum, tungsten or some special alloy. The size of the wire is about 5 μm in diameter and 1mm in length. It can have a resistance ranging from 10 Ω to 30 Ω and a temperature coefficient of resistance (TCR) about 0.1%/°C at room temperature. Such a wire would normally need a current from 10 to 40 mA to operate and a cut-off frequency of the anemometer in the tens of kHz range is obtainable using high speed electronics [2,3,4,5].

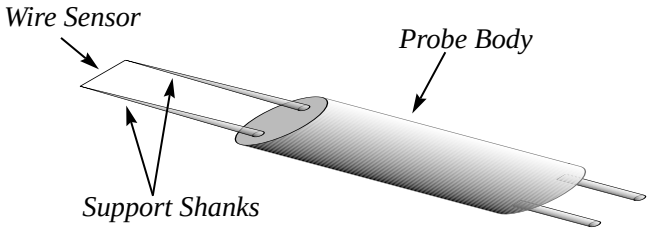

Figure 2.1 Schematic of conventional hot-wire probe.

Nevertheless, there is a major disadvantage of this type of hot wire anemometers; they need to be individually hand-assembled. This also means that it is difficult to build an array of wires for the simultaneous measurements of velocity distribution. In addition, because the wire dimensions do vary significantly, hot-wire probes are often not interchangeable without major re-calibration of the whole instrument.

As a result, to improve hot-wire anemometers, one can then look into three directions. First, future anemometers should be further down-sized. Since the spatial resolution of the anemometers for flow velocity distribution measurement is determined by its dimensions, it is advantageous if the wire size can be further reduced. This would also decrease power consumption and thermal interference to the flow and increase frequency response. However, the traditional technique can no longer make smaller hot wires with reasonable consistency. Second, techniques to build arrayed hot-wires should be developed. Third, new fabrication processes should avoid hand assembly and allow the mass production of the devices. Considering these requirements, our group then has conducted research on applying silicon micromachining technology to the manufacture of smaller and better hot-wire anemometers.

Silicon micromachining is a relatively new technology that is derived from VLSI technology [6] for making micro-electro-mechanical devices [7,8]. This is a proven technology for making chip-type or chip-supported free-standing-wire flow sensors [9,10,11,12]. Interestingly, though, no one has worked on micromachined hot-wire anemometers that possess the optimal features of a free wire in space without anything nearby except the two support shanks so that maximum thermal isolation and minimum

flow disturbance are obtained.

We present our work on the batch-fabricated and further down-sized hot wires that simulate the real structures of a conventional hot wire anemometer. Our hot wires are made with a new process that combines both surface and bulk micromachining technologies [13,14,15], and precisely doped low-pressure-chemical-vapor-deposited (LPCVD) polysilicon is used as the new wire material. Extensive electrical and wind-tunnel characterizations of these devices have been done and it is confirmed that these micron-sized hot wires do have much improved spatial resolution, sensitivity, and frequency response. In the following, we will discuss their design and fabrication, steady-state characteristics, dynamic characteristics, and directional dependency based on our experimental results.

2.2 Design and Fabrication

2.2.1 Structures and Materials

Our micromachined hot-wire anemometers have a structure similar to that of conventional hot-wire anemometers. It consists of a sensing wire, two parallel supports, a Si beam, and the thick Si handle, as shown in Figure 2.2. The Si beam acts as a thermal and mechanical buffer between the supports (0.5 μm thick) and the handle (500 μm thick) to avoid interference with the flow. The sensing wires are about 0.5 μm thick, 1 μm wide, 10-160 μm long, and are free standing to optimize the interaction with the flow and to minimize the thermal conduction to the handle. Heavily doped polysilicon, instead of platinum or tungsten, is used as the sensing and supporting material because of its compatibility with existing micromachining technologies and because of its good electrical and mechanical properties. For example, its Young's modulus is about 165 GPa and its TCR is 0.1-0.2%/^{o}C. The metal leads may extend all the way to the tips of the support shanks to reduce the voltage drop.

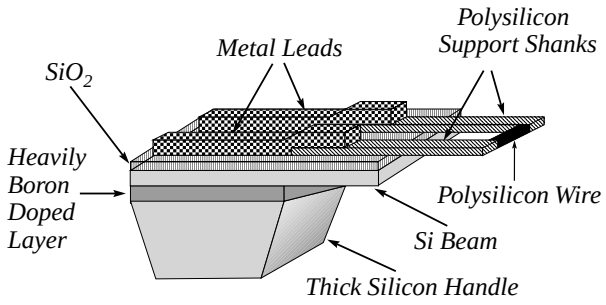

Figure 2.2 Schematic of the micromachined hot-wire probe.

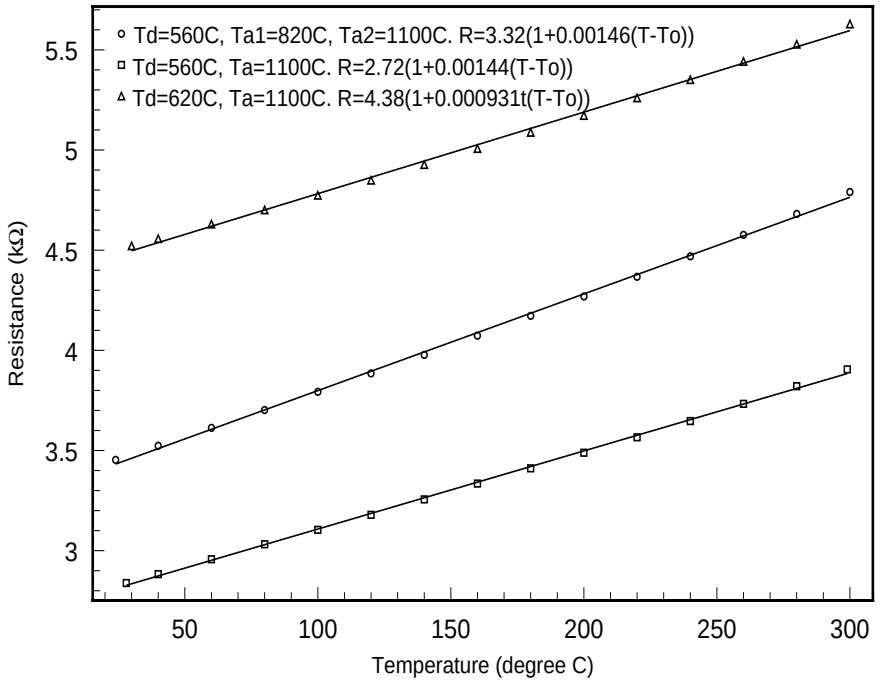

Figure 2.3 The temperature coefficient of boron doped ($2\times10^{20}cm^{-3}$) polysilicon resistors (50 squares) under different deposition and annealing conditions.

It has been reported that polysilicon, deposited in an amorphous state at low temperature and then crystallized at high temperature, has more controllable qualities than as-deposited polysilicon with the deposition temperature at 620^{o}C [16]. We choose to use the former polysilicon, and its electrical properties were calibrated before the fabrication of our anemometers. It is found that the TCR is about 50% higher and the resistance-temperature characteristic is more linear than the normal polysilicon

(deposited at 620^{o}C) at a doping concentration of 2×10^{20} cm^{-3}, as shown in Figure 2.3. Moreover, the stress distribution in this polysilicon along the depth is much more uniform, as we will see from the SEM picture in the discussion section. The calibration results also show that 2×10^{20} cm^{-3} is the doping concentration which gives the lowest sheet resistivity (resistivity divided by film thickness) of 30 Ω/square and highest positive TCR, and therefore, is the optimum doping concentration for hot wires.

2.2.2 Fabrication Process

Two generations of anemometers have been fabricated at the Caltech Micromachining Lab. The first generation has silicon nitride encapsulating the polysilicon wire and support shanks. The polysilicon wires of the second generation are directly exposed to air and consequently the frequency response is improved by an order of magnitude. Figure 2.4 is the simplified fabrication process flow with cross-sections. The detailed process steps are listed in Appendix A.

The fabrication process starts with the deposition of 0.2 μm low-stress silicon nitride and 2 μm low temperature silicon dioxide (LTO) on (100) Si wafers with a 70 μm lightly doped epitaxial layer on top of a 8 μm heavily boron-doped etch stop layer. A 0.6 μm thick amorphous Si layer is deposited at 560^{o}C and doped by boron ion implantation with a dose of 1×10^{16} cm^{-2} at energy of 80 keV. Annealing is done at 1100^{o}C, followed by the patterning of polysilicon by Reactive Ion Etching (RIE). This results in 0.5 μm thick polysilicon resistors with a uniform boron concentration of 2×10^{20} cm^{-3}. After the aluminum or gold metallization, a 3 μm LTO is deposited at 450^{o}C, and the front-side and backside Si substrate windows are opened using both wet and dry (plasma) etchings. A 10 hour EDP anisotropic etching at 95^{o}C removes the Si underneath the polysilicon probe. Finally, RIE etching and pad etchant are used to strip the heavily doped boron layer, nitride and LTO layer respectively. Figure 2.5 shows the SEM pictures of the tips of some hot-wire anemometers fabricated using this process, and Figure 2.6 is the photograph of the tilted devices, which corresponds to the sketch in Figure 2.2.

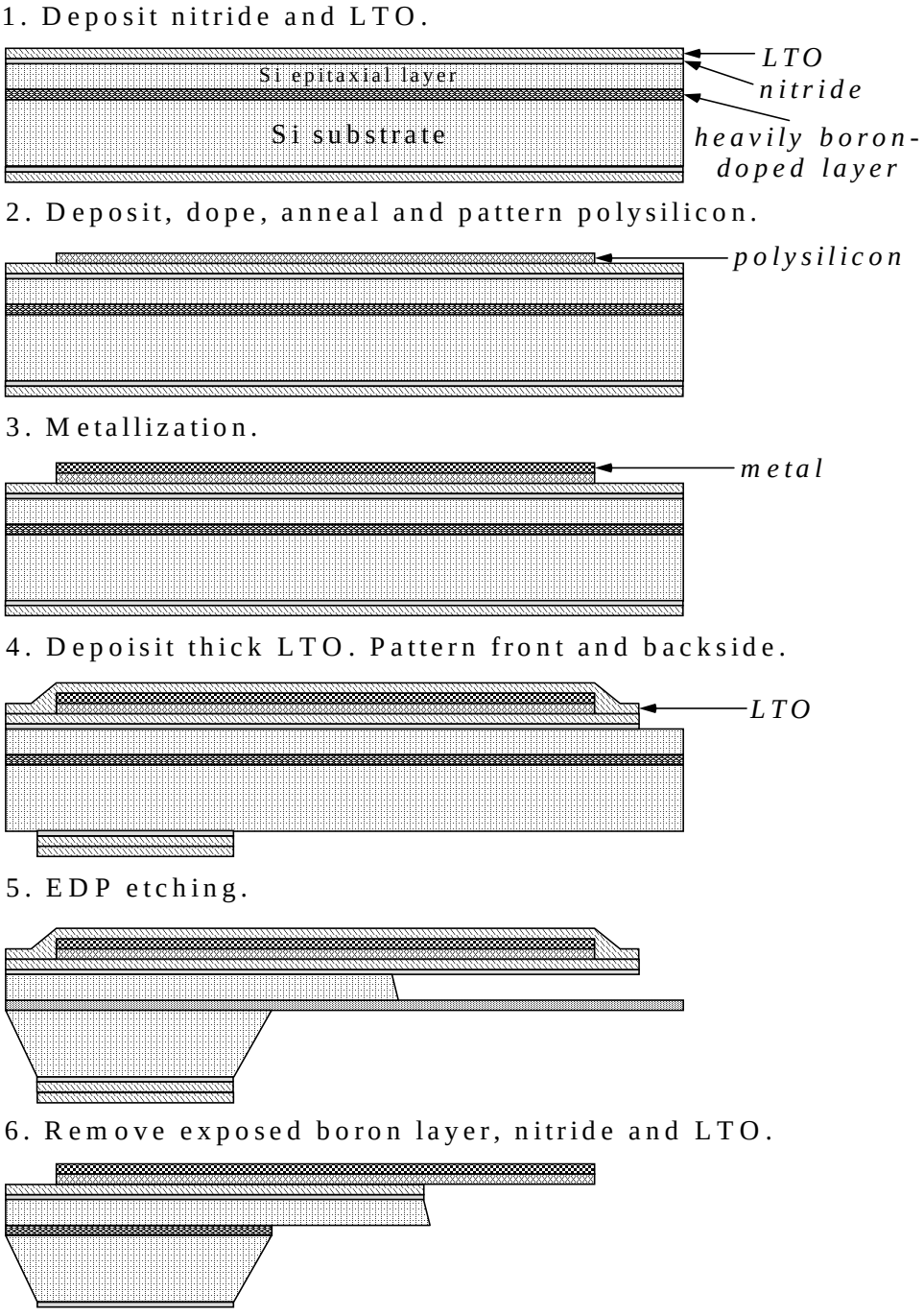

Figure 2.4 Simplified process flow with cross-sections for the fabrication of the micromachined hot-wire anemometers.

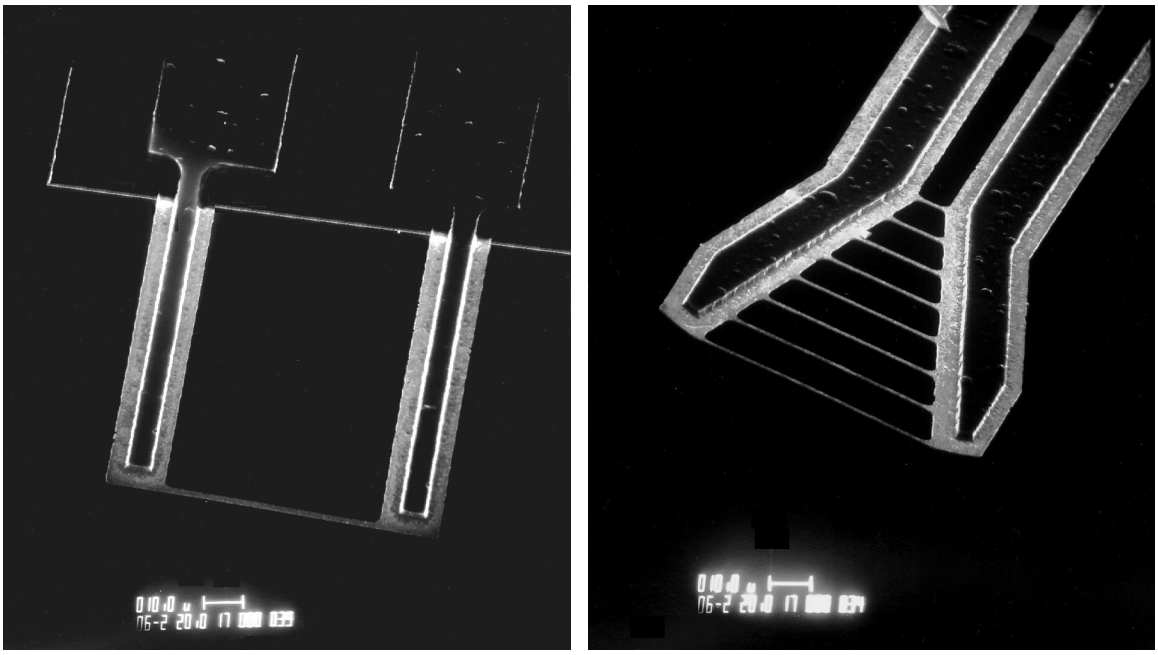

(a) (b)

Figure 2.5 SEM pictures of (a) a 70 μm long hot wire and (b) a multiple-wire probe.

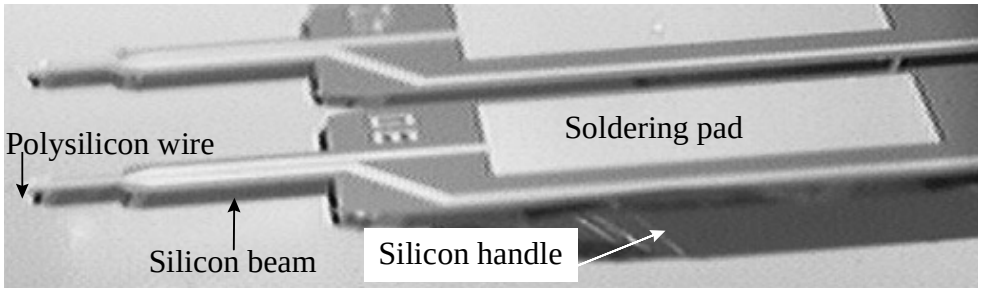

Figure 2.6 Photograph of tilted hot wires.

2.2.3 Corner Compensation

It is worthwhile to discuss more about the Si anisotropic etching used in this process. The convex corners of a single crystal silicon structure consist of crystallographic planes with different orientations. Among them, the (211) plane has the fastest etching in Si isotropic etchants such as EDP and TMAH. As a result, the convex corners is undercut at a significant rate and the final structure may be very different from what has been designed. The solution is to add compensation structures to the corners on the mask to

delay the formation of convex corners on the real structures to the last minute of the etching. Typical compensation structures include squares and long beams. Their dimensions are determined by calibration. Basically, a wide structure can stand longer etching.

In the layout design of the hot wires, we have included the corner compensation structures shown in Figure 2.7. On the backside, they are wide and long straight beams and stand more than 10 hours of etching in EDP or TMAH for the designed structures to be formed. On the front side, they are 80 μm wide and 2000 μm long folded beams and can stand slightly longer time of etching. The etching is stopped as soon as the compensation structures on the front side are consumed completely.

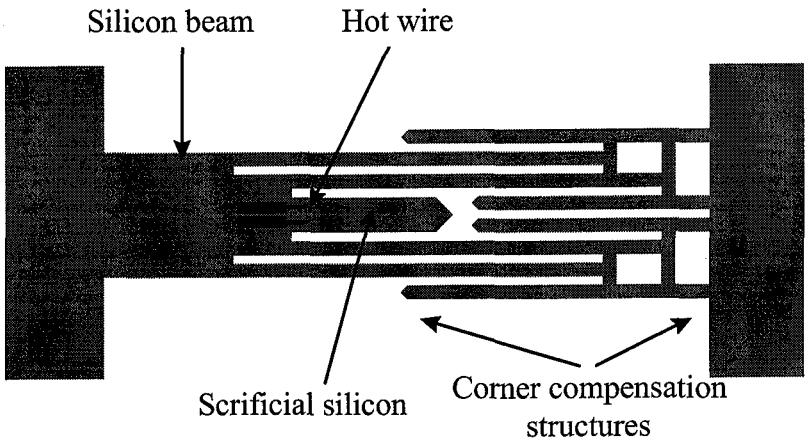

Figure 2.7 Long corner compensation structures on the front side for a 10 hour or more EDP etching.

The above corner compensation scheme works well if the Si isotropic etching is repeatable and uniform. In reality, it is not always the case. For example, the etching properties of EDP, including the etching rate and the ratio of etching rates for different crystallographic planes change as the solution gets aged. TMAH is better, but is still far from ideal. To make the fabrication process more robust, the front and back side etchings need to be separated. For example, pattern and etch the back side; deposit chrome or gold to protect back side; Pattern and etch front side. This way, the corner compensation

structures on the front side can be much shorter, thus greatly reducing the bad effect of non-uniform etching.

2.2.4 Packaging

After the fabrication process is finished, each individual probe is connected to the wafer frame or other probes by four 70 μm thick narrow Si beams and can be easily separated by hand without causing damage to the delicate probes. The package of the anemometers is a ceramic tube a few centimeters long and 3 mm in diameter. The anemometer handle is soldered with electrical cables, placed inside the tube and then epoxy-fixed. During handling, all mechanical vibrations are avoided so as not to damage the wires. Figure 2.8 shows the prototype of a packaged anemometer. This is, of course, the very preliminary packaging scheme for laboratory testing purpose only. More delicate packaging can be developed, such as using thermal compression wire bonding, etc..

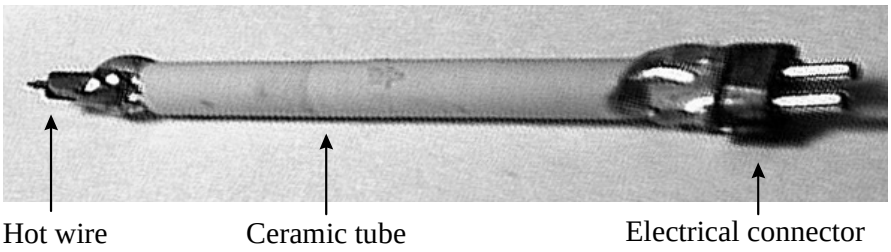

Figure 2.8 Prototype of packaged hot wires.

2.3 Steady-State Characteristics

2.3.1 Operation Modes and Operating Points

Traditionally, there are two operation modes for hot wires. One is the constant current (CC) mode and the other is the constant temperature (CT) mode. The CC bias circuit is very simple and always stable due to the lack of feedback. It does not generate much noise in the output. However, its low frequency response (only a few hundred Hz for

conventional hot wires) has limited its use to very few occasions. CT bias, on the other hand, uses the most advanced feedback electronics to achieve high frequency response. It is the dominating operation mode of practical hot wire anemometers, even though the circuit is less stable and more noisy. However, for our new micromachined hot wires, it is important that we investigate their characteristics in both CC and CT modes because this would help us understand the new hot wires more completely.

The acceptable operating temperature range of hot wires determine the operating points. The wire has to be heated up to certain temperature well above the ambient in order to have reasonable sensitivity to velocity. However, that temperature can not be too high so as to burn the wire or cause deterioration and constant drift in material properties. For polysilicon, the operating temperature should be kept below 250^{o}C, even though its melting temperature is around 1400^{o}C. Therefore, a reasonable operating temperature range of our hot wires in air should be 100 - 250^{o}C, which corresponds to resistance over-heat ratios (defined as $a_R = \frac{R - R_a}{R_a}$, where R is the wire resistance at the operating temperature, R_a is the wire resistance at the ambient temperature) of 0.15 - 0.35.

2.3.2 Sensitivity to Velocity

The steady-state characteristics of hot wires with lengths between 20-160 μm have been measured in wind-tunnels. For example, Figure 2.9 and Figure 2.10 are the responses of an 80 μm long hot-wire anemometer at different over-heat ratios without any electronic gain in CC and CT modes, respectively. As a comparison, Figure 2.11 gives the responses of a conventional hot wire 1 mm in length and 5 μm in diameter in CC mode. The two types of hot wires needs about 2-3 mW and 4-8 mW respectively to reach the over-heat ratios of 0.15-0.35. The significantly smaller power consumption of our hot wire is mainly due to its smaller size. Furthermore, our hot wire only needs less than 1.5 mA of bias current, while the conventional hot wire needs more than 10 mA. This is because our hot wire has much higher resistance as well as smaller size (less power).

Since almost all commercial operational amplifiers can supply a few mA of current, the current booster used in most conventional hot wire anemometer circuits can be omitted for our hot wire. Finally, and most importantly, our hot wire is more sensitive than the conventional one. This is simply because the output voltage is proportional to the square root of wire resistance, i.e., $V = \sqrt{PR}$, when the total power P is given.

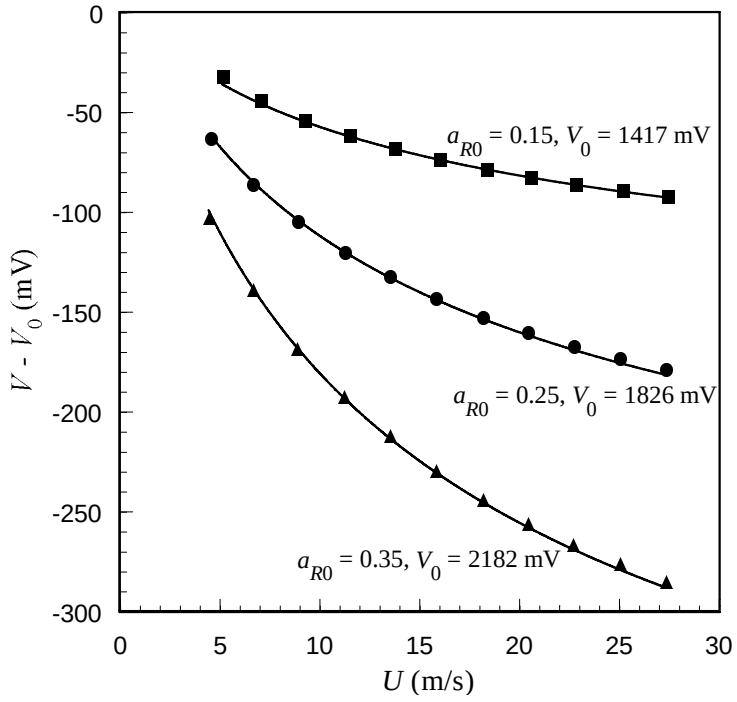

Figure 2.9 Output characteristics of a 80 μm long hot wire in CC mode.

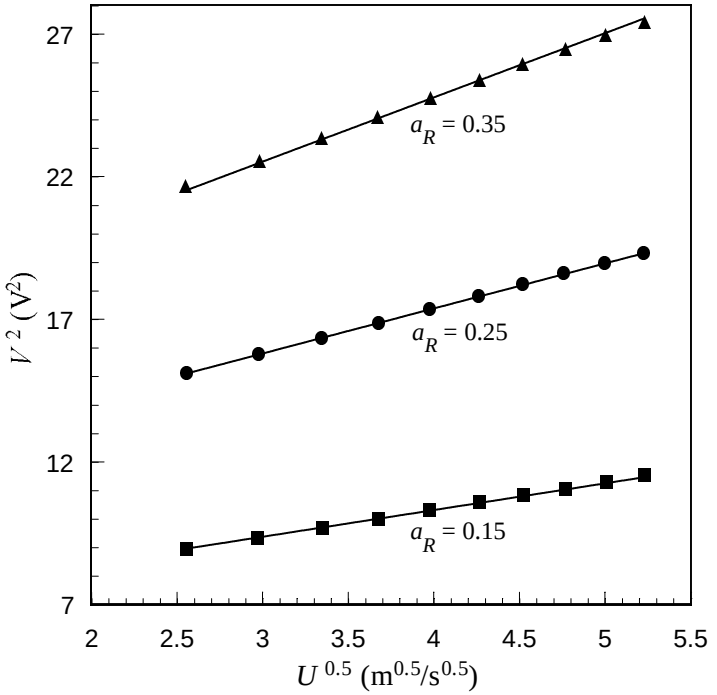

Figure 2.10 Output characteristics of the 80 μm long hot wire in CT mode.

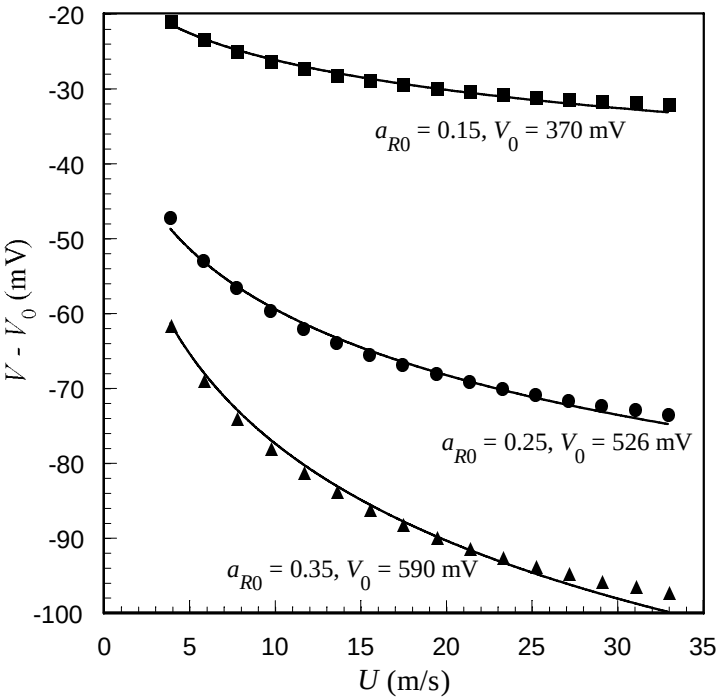

Figure 2.11 Response of a conventional hot wire (5 μm in diameter, 1mm in length) in CC mode. The currents are 10 mA, 13 mA and 14 mA respectively for over-heat ratios of 0.15, 0.25 and 0.35.

Figure 2.12 shows the absolute and normalized output voltages at a flow velocity of 27 m/s for hot wires with lengths from 20 μm to 160 μm in CT mode with a_R = 0.25. It is obvious that longer (larger aspect ratio) hot wires are more sensitive than shorter ones. This is one of the reasons why conventional hot wires always have large aspect ratio (> 200). However, for the micromachined hot wires, even the short ones have reasonable sensitivities. For example, the output of a 20 μm long hot wire in CT mode at a velocity of 27 m/s is about 200 mV. According to the trend of the data in Figure 2.12, the output for a 10 μm hot wire should be over 100 mV. Unfortunately, the experimental data is not available for hot wires of this length.

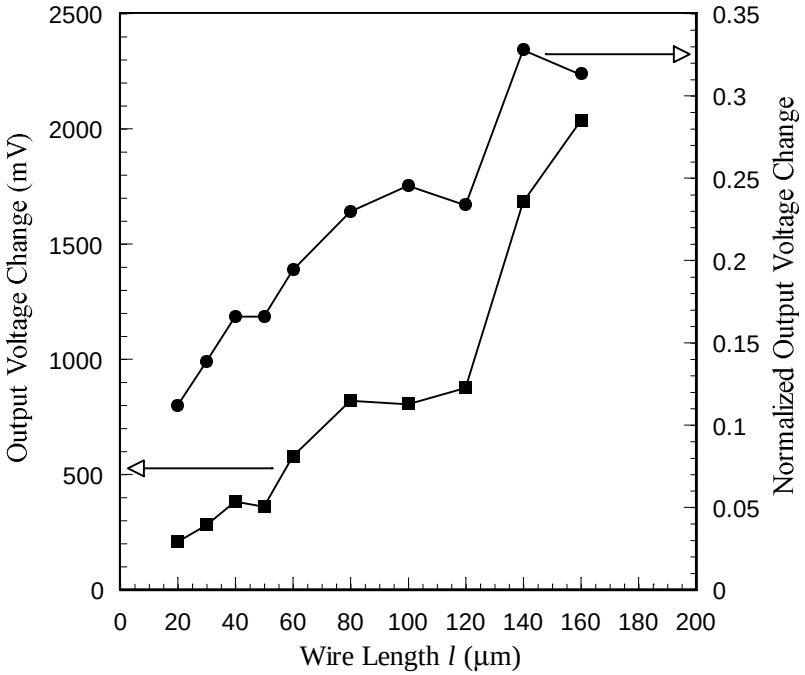

Figure 2.12 Output voltages at the air flow velocity of 27 m/s for hot wires with different lengths in CT mode.

2.3.3 King's Law

To interpret the above experimental results, we have to work out the theoretical relationship between the hot wire output and flow velocity using heat transfer theory. In

steady state, power generation and heat dissipation of a hot wire is balanced, i.e.,

$$P = \frac{V^2}{R} = K_{eff}(U)(T - T_a) \qquad (2.1)$$

where R is the wire resistance, V is the voltage across the wire, T is the average wire temperature, T_a is the ambient temperature, U is the flow velocity, and $K_{eff}(U)$ is the effective heat transfer coefficient. In a laminar flow, King's law applies,

$$K_{eff}(U) = K_0 + K_1 U^n \qquad (2.2)$$

where K_0 is the heat transfer coefficient which takes into account conduction, radiation and free convection and is not a function of U, and $K_1 U^n$ represents forced convection by the boundary layer flow. The exponent n depends on the hot wire structure and is approximately 0.5 for conventional hot-wire anemometers.

Assuming linear change of wire resistance with temperature, we have

$$R = R_0[1 + \alpha_R(T - T_0)] \qquad (2.3)$$

where R_0 and α_R are the resistance and the temperature coefficient of resistivity (TCR) at the reference temperature T_0. Therefore,

$$T - T_a = \frac{R - R_a}{\alpha_R R_0} \qquad (2.4)$$

and Eq. (2.1) becomes

$$\frac{V^2}{R} = K_{eff}(U)\frac{R - R_a}{\alpha_R R_0} \qquad (2.5)$$

In CC mode, the current is kept constant. Therefore,

$$\frac{V}{R} = \frac{V_0}{(1 + a_{R0})R_a} \qquad (2.6)$$

where V_0 and a_{R0} are the output voltage and over-heat ratio at $U = 0$, respectively. The following expression for K_0 can be derived from Eq. (2.5) at $U = 0$,

$$K_0 = \frac{\alpha_R R_0 {V_0}^2}{a_{R0}(1+a_{R0}){R_a}^2} \tag{2.7}$$

This equation means that, for a given K_0 and a_{R0}, the voltage is larger for higher resistance wires. Combining Eqs. (2.5)-(2.7), it is easy to show that

$$V = \frac{1+AU^n}{1+(1+a_{R0})AU^n}V_0 \tag{2.8}$$

or

$$V - V_0 = -\frac{a_{R0}AU^n}{1+(1+a_{R0})AU^n}V_0 \tag{2.9}$$

where $A = \frac{K_1}{K_0}$. Eq. (2.9) shows that the output voltage of a hot wire with positive TCR decreases with increasing flow velocity. The higher the over-heat ratio, the faster the decrease.

In CT mode, R is kept constant and Eq. (2.5) can be written as

$$V^2 = (1 + AU^n){V_0}^2 \tag{2.10}$$

Usually, the circuit in Figure 2.13 is used to realize the CT operation and the voltage across the Wheatstone bridge V_{out}, rather than the voltage across the hot wire V, is measured. Then,

$$V_{out} = \beta V = \beta(1+AU^n)^{\frac{1}{2}}V_0 \tag{2.11}$$

where $\beta = 1 + \frac{R_2}{R_3}$ is the bridge gain.

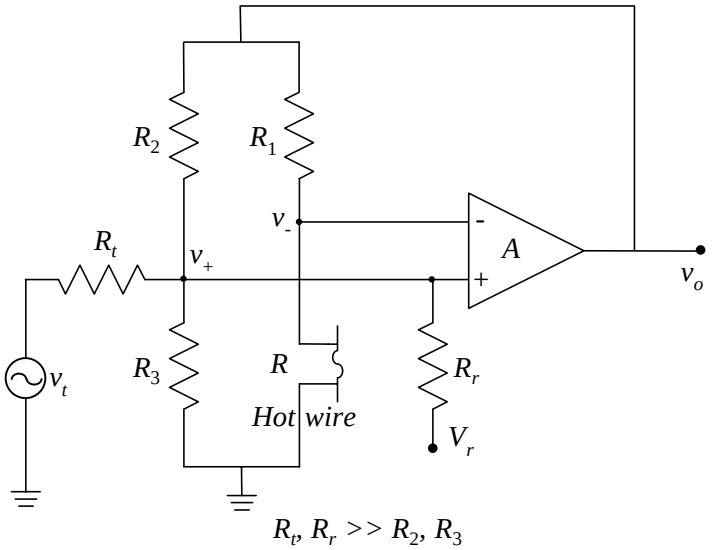

Figure 2.13 Simplified constant temperature bias circuit.

Eqs. (2.8) and (2.11) have been used to fit the experimental data in Figs. 2.9-2.11. The ratio of K_1 to K_0, i.e., the constant A in Eqs. (2.8) and (2.11) is found to be 0.10 for the micromachined hot wire and 0.15 for the conventional hot wires. This means that the conventional hot wire has higher percentage of total heat being convected to the flow than the micromachined one. It is simply because the conventional hot wire has much higher aspect ratio and hence less conduction loss to the support needles. On the other hand, the fitted value of the exponent n to velocity U for our hot wire and for the conventional hot wire in CC mode are 0.77 and 0.50 respectively. Thus, in comparison with the conventional hot wire, our hot wire has a more linear response and less degradation in sensitivity in the high velocity regime than the conventional anemometer. Previously [17], we suspected that the unusual n value for our hot wire might be caused by the non-circular cross section of our hot wire [18]. However, n and A for the micromachined hot wire in CT mode has been found to be 0.50 and 0.143, respectively. Then the question is that which fitted value truly represents the exponent n to velocity U in King's law. In order to answer this question, we need to re-examine the fitting equations and the fitting process. We considered A to be not a function of the flow velocity. This assumption stands for hot wires with larger aspect ratios, where K_0 and K_1 are independent of wire

temperature, or, for hot wires in CT mode, where the wire temperature is kept constant. However, for hot wires with small aspect ratios in CC mode, significant conduction heat loss to the supports exists, which in turn causes non-uniform temperature distribution along the wire. K_0 and K_1 may thus depend on the wire temperature, which changes with flow velocity in CC mode. This effect may have been reflected through the different fitting values of n in CC and CT modes.

2.4 Dynamic Characteristics

2.4.1 Time Constant Measurement

In addition to steady-state response, dynamic response of an anemometer is also important especially for large Reynolds number flow measurements. In fact, the greatest advantage of the micromachined hot wires should be their improved bandwidth due to their extremely small sizes or low thermal masses.

The time constant can be determined by superimposing a small signal (square wave or sine wave) on a constant bias current. Figure 2.14 shows the CC bias circuit that we used to measure our hot wires. The square wave is used if the hot wire has only one thermal time constant. This is often true for hot wires with aspect ratios larger than 200 [4]. For example, Figure 2.15 shows the square-wave response of a hot wire with aspect ratio of 200. The slow increase or decrease following the abrupt jump in the output is the thermal delay. τ is simply the time duration for the output change due to the thermal effect to reach 63% of its total, as shown in Figure 2.15.

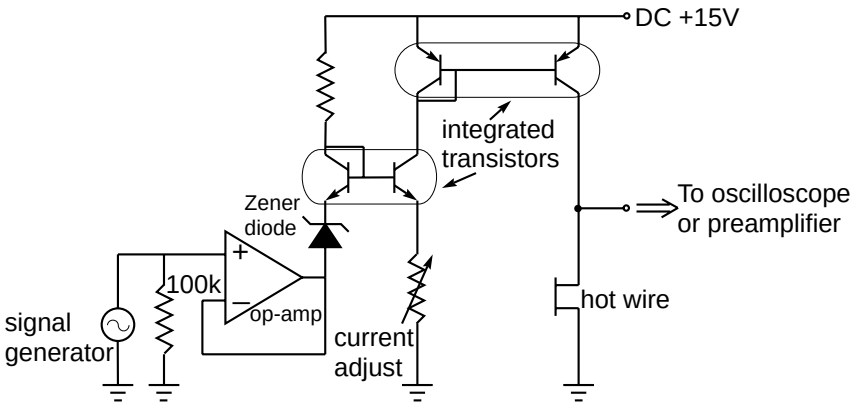

Figure 2.14 The constant current anemometer circuit for time constant measurement and wind-tunnel testing.

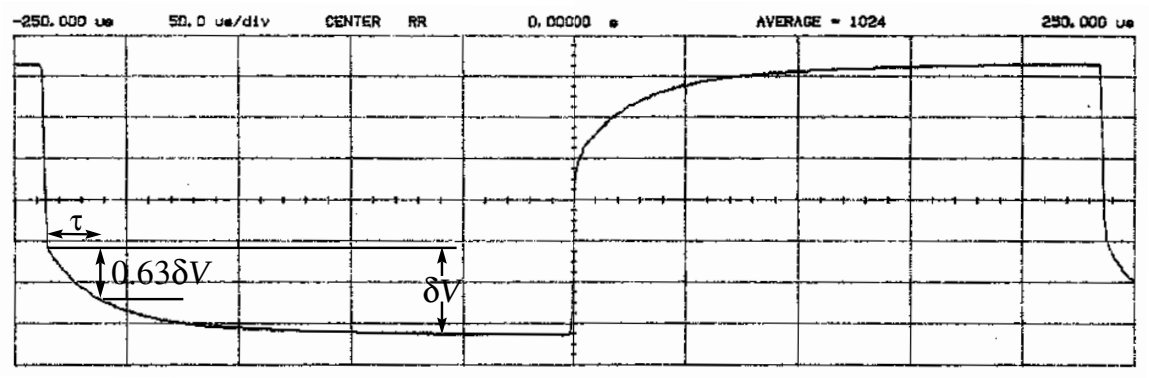

Figure 2.15 Square wave response of a 200 μm long hot wire in CC mode.

On the other hand, if the aspect ratio of a wire is less than 200, its thermal response may have two time constants. One (τ_2) is associated with the sensing wire and the other (τ_1) with the wire support shanks. In this case, the square-wave method may not be accurate, and using sine wave signals to do the measurements in the frequency domain is suggested. Figure 2.16 shows the measured total resistance of a 10 μm long wire as a function of frequency. Since the two time constants are different by more than an order of magnitude, this resistance can be accurately modeled by,

$$r = R + \frac{r_1}{1 + s\tau_1} + \frac{r_2}{1 + s\tau_2} \tag{2.12}$$

where R is the dc resistance, r_1 and r_2 are the amplitudes of the resistance change caused by ac heating effects. Fitting Eq. (2.12) into the experimental data in Figure 2.16 then gives the two thermal time constants. For our hot wires, the ratio of r_2 to r_1 increases with the wire length l. The time constant associated with the support shanks, τ_1, always ranges between 100 μs and 300 μs because of the fixed geometry design.

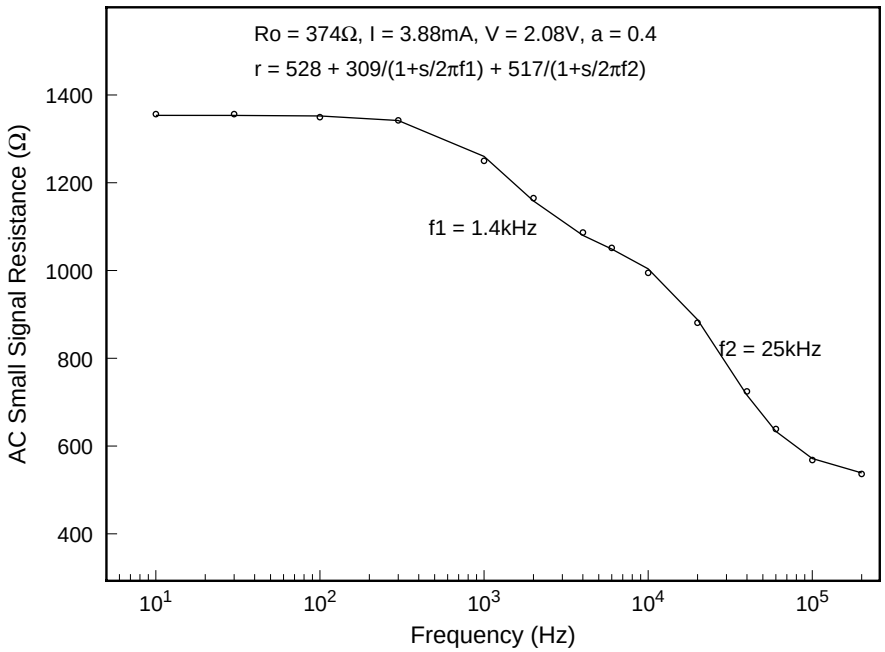

Figure 2.16 AC resistance change of a 10 μm long hot wire in the frequency domain.

2.4.2 Transient Analysis

In principle, the heat transfer is a three-dimensional problem. However, because the dimension of the wire in x direction is much larger than those in y and z directions, we can reasonably assume that temperature is not a function of y and z and the problem is simplified to a one-dimensional heat transfer.

For a wire with length l, width w and thickness d at some time t and position x from one end (see Figure 2.21), the sum of the heat absorbed by a unit length wire and the heat flowing into it through thermal conduction and convection in unit time must be equal to the ohmic heat [19], i.e.,

$$\rho w d c_p \frac{\partial T}{\partial t} - \kappa_{poly} w d \frac{\partial^2 T}{\partial x^2} + 2h(w+d)(T - T_a) = J^2 \rho_0 w d[1 + \alpha_R (T - T_0)] \quad (2.13)$$

where ρ = 2.32 g/cm^3, c_p = 0.7 J/(g·^{o}C), ρ_0 and κ_{poly} are the density, specific heat, resistivity, and thermal conductivity of polysilicon, respectively, J is the current density, and h is the convective heat transfer coefficient of the wire. The above differential equation can be solved with the boundary conditions $T(0,t) = T(l,t) = T_a$ and initial condition $T(x,0) = T_a$, assuming that the two support shanks are perfect heat sinks. The solution is a multiple-mode response. The first mode determines the time constant,

$$\tau_2 = \tau_{21}\tau_{22} / (\tau_{21} + \tau_{22}) \quad (2.14)$$

with

$$\tau_{21} = \frac{\rho c_p}{-\alpha_R J^2 \rho_0 + \frac{2h(w+d)}{wd}} \quad (2.15)$$

and

$$\tau_{22} = \left(\frac{l}{\pi}\right)^2 \frac{\rho c_p}{\kappa_{poly}} \quad (2.16)$$

It can be seen from the above expressions that the time constant is due to two components: convection time constant τ_{21}, which dominates for long wires, and conduction time constant τ_{22}, which dominates for short wires.

The measured τ_2 for our wires with lengths from 20 μm to 160 μm is shown in Figure 2.17 with the theoretical fitting from Eq. (2.14). h = 0.65 W/(cm^2·^{o}C) and κ_{poly} = 0.26W/(cm^2·^{o}C) (0.34W/(cm^2·^{o}C) reported by Tai et al. [20]) are the fitting parameters. It is clear that when l is small, the conduction time constant τ_{22} dominates and that τ_2 increases parabolically with l. If l is large, the convection time constant τ_{21} dominates and τ_2 becomes a constant. As expected, the shortest wire (10 μm long) gives the smallest τ_2 of 4 μs. This corresponds to a bandwidth of 40 kHz, which is a significant improvement over conventional hot wires (typical bandwidth of 700 Hz).

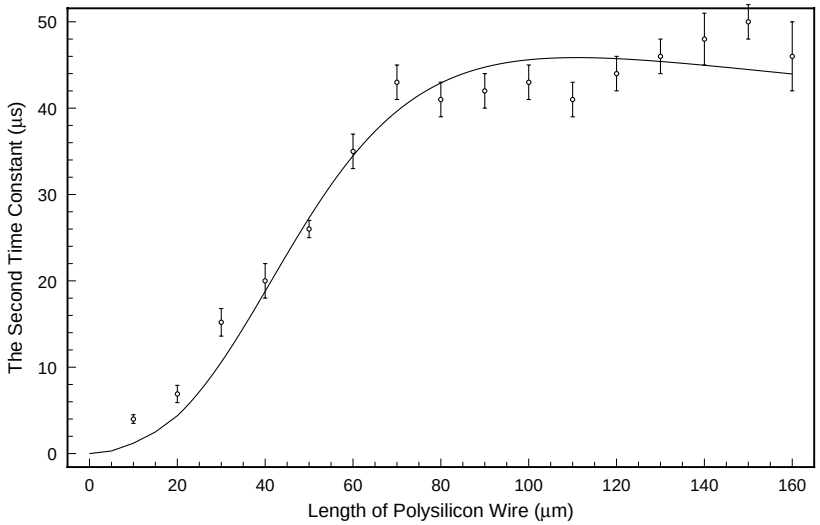

Figure 2.17 Time constant in CC mode of the micromachined hot wires with different wire lengths.

2.4.3 Constant Temperature Operation

Since the constant temperature operation of hot wires involves negative feedback, it significantly improves the frequency response over the CC mode. Figure 2.13 shows the circuit for our CT frequency response measurement. It is basically a Wheatstone bridge with a feedback operational amplifier. The ratio between R_2 and R_3 determines the dc gain, while R_1 is used to adjust the over-heat ratio or operating temperature of the hot wire. R_r and V_r are introduced here to adjust the stability of the circuit, i.e. the quality factor Q in this second-order system. The characteristic equations for the hot wire, the operational amplifier and the bridge are as follows,

$$\tau \frac{d\Delta R(t)}{dt} + \Delta R(t) = ai(t) + bu(t) \tag{2.17}$$

$$M \frac{dv_o(t)}{dt} + v_o(t) = A_0 v_i(t) \tag{2.18}$$

$$v_i(t) = -\frac{R_2 R_3 V_r}{(R_2 + R_3) R_r \overline{V_o}} v_o(t) - \frac{R_1 \overline{V_o}}{(R_1 + \overline{R})^2} \Delta R(t) - \frac{R_1 \overline{R}}{(R_1 + \overline{R}) R_t} v_t(t) \tag{2.19}$$

$$i(t) = \frac{v_o(t)}{R_1 + \overline{R}} - \frac{\overline{V_o}}{(R_1 + \overline{R})^2} \Delta R(t) + \frac{R_1}{(R_1 + \overline{R}) R_t} v_t(t) \tag{2.20}$$

where $\Delta R(t) = R(t) - \overline{R}$, $a = 2a_R \overline{R}(R_1 + \overline{R}) / \overline{V_o}$, $i(t)$ is the current through the hot wire, $u(t)$ is the flow velocity fluctuation, M and A_0 are the time constant and dc open loop gain of the operational amplifier. The output voltage $v_o(s)$ in frequency domain can be derived from these characteristic equations,

$$v_o(s) = \frac{G_v(1 + \frac{s}{\omega_1}) v_t(s) + S_u u(s)}{1 + \frac{s}{Q\omega_2} + (\frac{s}{\omega_2})^2} \tag{2.21}$$

where

$$\omega_1 = \frac{1}{(1 + 2a_R)\tau} \tag{2.22}$$

is the frequency at the system zero,

$$\omega_2 = \sqrt{\frac{2a_R A_0}{M\tau} \frac{R_2 R_3}{(R_2 + R_3)^2}} \tag{2.23}$$

is the natural frequency of the system,

$$Q = \frac{(R_2 + R_3) R_r}{R_2 R_3} \frac{\overline{V_o}}{V_r} \frac{M\omega_2}{A_0} \tag{2.24}$$

is the quality factor and can be adjusted by varying V_d,

$$G_v = (1 + \frac{1}{2a_R}) \frac{R_1 + \overline{R}}{R_t} \tag{2.25}$$

is the dc gain to the electrical testing signal v_t, and

$$S_u = \frac{b\overline{V_o}}{2a_R\overline{R}} \tag{2.26}$$

is the sensitivity to flow velocity signal. The system is normally biased into the critical damping state by adjusting Q to 0.5 to maximize the usable bandwidth.

According to Eq. (2.21), if the response to the electrical signal v_t is measured, the response to the velocity signal u can be predicted. Therefore, the electrical signal v_t is often used to calibrate the dynamic response of CT anemometers as sine or square wave velocity signals are difficult to obtain experimentally. However, when doing velocity measurements, the electrical signal must be disconnected. It is worth noting that the gain-bandwidth product of the operational amplifier can limit the bandwidth of the overall circuit. To maximize the bandwidth, a high speed operational amplifier should be used.

In the case that a hot wire has two time constants, the CT anemometer will behave as a third-order system. This will make frequency response measurement and analysis much more difficult. Fortunately, our anemometers always have r_2/τ_2 much larger than r_1/τ_1 (at least by an order of magnitude) so that Eqs. (2.21-2.23) can still be used with τ replaced by τ_2.

As an example, LM6365, a very high speed operational amplifier with gain-bandwidth of 700 MHz is used with a 10 μm long hot wire to constitute an CT anemometer system. The resistance ratio of R_2 to R_3 is set to one. The over-heat ratio is adjusted to 0.3. Figure 2.18 shows the measured frequency response to v_t together with its theoretical fitting curve and the calculated response to velocity signal from Eq. (2.21). System bandwidth of 1.4 MHz is identified. This is further verified by the square-wave response shown in Figure 2.19 where the bandwidth is approximately $1/(1.3t_1)$=1.4 MHz, with t_1 = 0.5 ~ 0.6 μs as the peak width of the response curve [4]. Furthermore, Eq. (2.23) can be used to calculate the bandwidth. The result is 1.6 MHz, which is in good agreement with the measured value.

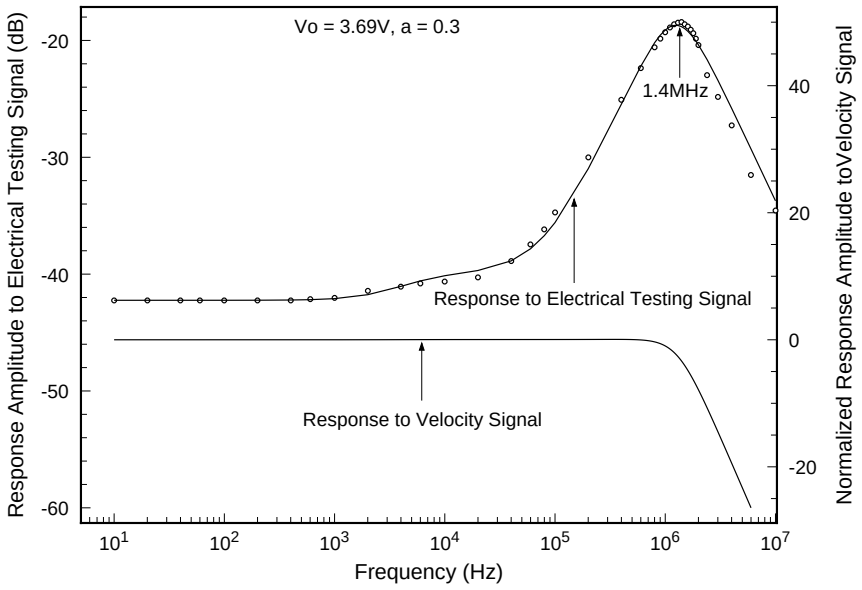

Figure 2.18 Frequency response of a 10 μm long hot wire in CT mode.

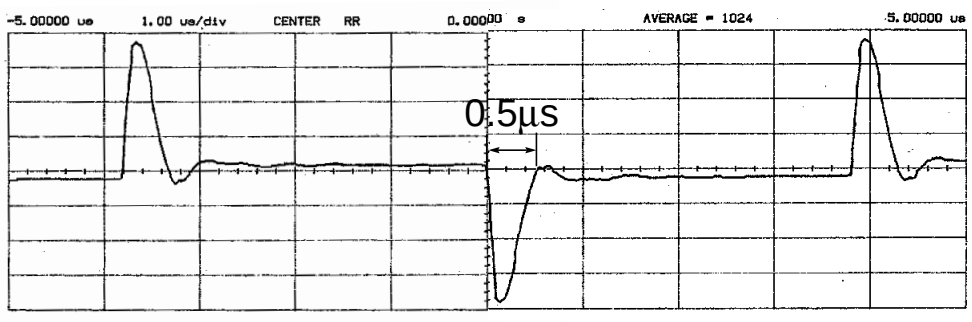

Figure 2.19 Square wave response of the 10 μm long hot wire in CT mode.

Finally, Figure 2.20 shows the bandwidth of hot wires with different lengths. The bandwidths for the hot wires with large aspect ratios are around 500 kHz. During the measurement, we noticed that the circuit stability is very sensitive to the stray capacitance of long cables connecting the hot wires to the circuit, due to the high resistance of the wires. A small capacitor may be added in parallel with R_1 to suppress the oscillation. However, in some cases, the bandwidth is degraded.

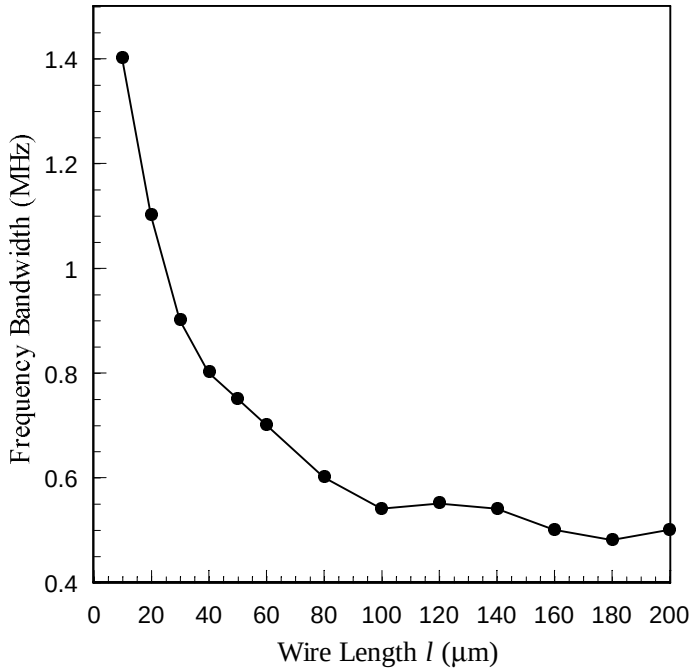

Figure 2.20 Frequency bandwidths of the micromachined hot wires with different lengths in CT mode.

2.5 Directional Dependency

Directional dependency is essential if an anemometer is used to determine velocity vectors. For hot-wire anemometers, the output characteristics depend on yaw angle and pitch angle, but not on roll angle. As defined in Figure 2.21, the yaw angle θ is the angle between the velocity vector U and its transverse component normal to the wire , and the pitch angle ϕ is between U and the hot wire probe body axis y.

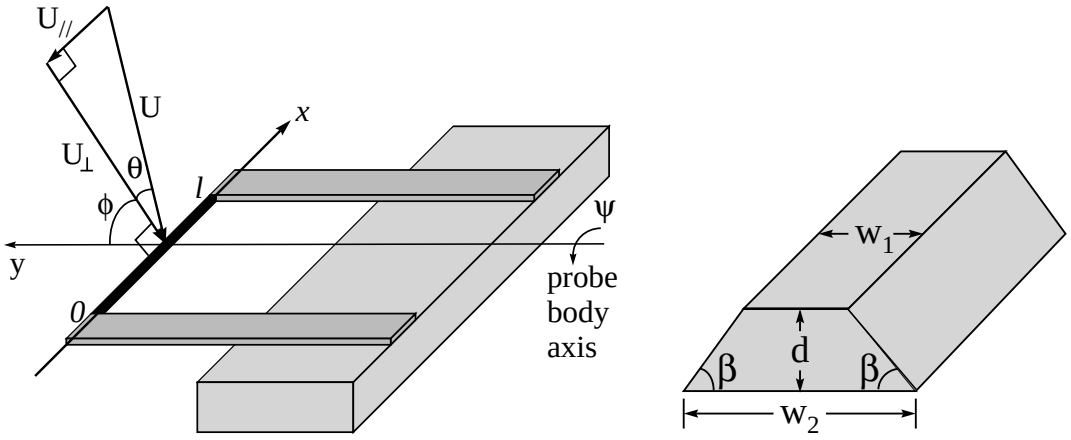

Figure 2.21 (a) Definition of yaw angle θ, pitch angles ϕ and roll angle ψ. (b) Cross section of micromachined hot wires.

For large aspect-ratio hot wires, the transverse velocity component $U_t = U\cos\theta$ is mainly responsible for wire cooling by convection. A cosine response to the yaw angle θ is then expected. This dependency is observed for an 160 μm long hot wire in CT mode, as shown in Figure 2.22. The sharp voltage drop for the yaw angle higher than 90^o is because the wire is already in the wake of the probe body. On the other hand, for small aspect-ratio hot wires such as a hot point sensor, there should be no directional dependency. Therefore we do not expect strong yaw angular dependency of the output for a small aspect-ratio hot wire. This is also confirmed in Figure 2.23 for a 20 μm long hot wire. Interestingly, at low velocity, the output voltage increases with θ. This is because the longitudinal velocity component parallel to the wire, U_l, contributes more to the wire cooling through the convection assisted heat conduction along the wire than U_t.

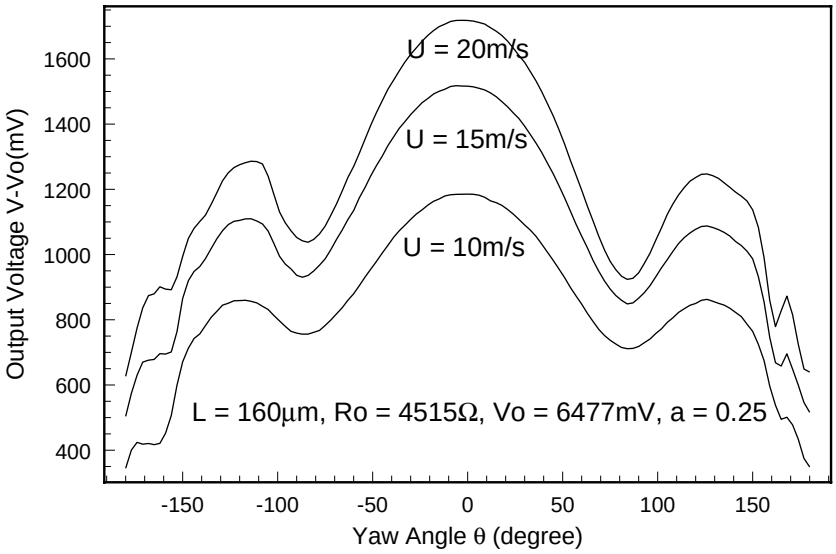

Figure 2.22 Yaw angular dependency of a 160 μm long hot wire in CT mode.

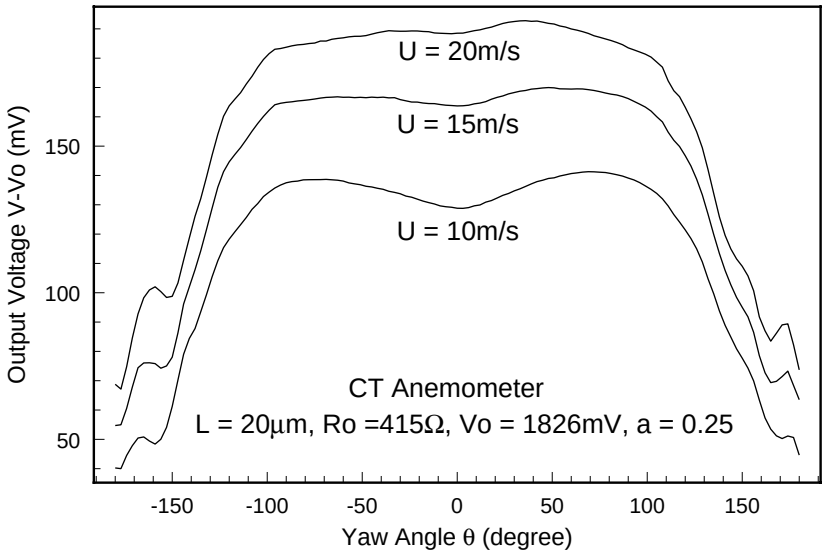

Figure 2.23 Yaw angular dependency of a 20 μm long hot wire in CT mode.

The pitch angular dependency of a hot wire can be attributed to three effects [21]. The first one is the hydrodynamic effect of the fluid passing through the opening bounded by the wire, support shanks, and the probe body when the pitch angle is increased. The second one is the additional cooling of the support shanks because they are oriented

broadside to the flow during pitching. This effect is especially significant for shorter wires since more heat loss is through the support shanks. The third one is the varying effective cooling surface area during pitching. The first two effects tend to increase the cooling, while the third one depends on the wire geometry. For conventional hot wires, which are cylinders with large aspect ratios, only the first effect exists and causes 10 to 20 percent change in output during pitching. However, for micromachined hot wires all three effects are significant due to the special structural design and the trapezoidal wire cross section (Figure 2.21(a)). Therefore we expect strong pitch angular dependency for these hot wires, especially when *l* is small.

Figure 2.24 and Figure 2.25 are the measured pitch angular dependencies of the same hot wires used in Figure 2.22 and Figure 2.23. The 20 μm long hot wire has much stronger pitch angle dependence than the 160 μm long one. This strong pitch angular dependency is useful for such a short wire because the yaw angular dependence is small. We noticed that the pitch characteristics are not symmetrical. One of the maxima occurs at $\phi = -90^o$ (when air flow blows toward the bottom of the wire), while the other one occurs at $\phi = 60^o \sim 70^o$. We believe this is due to the trapezoidal wire cross section.

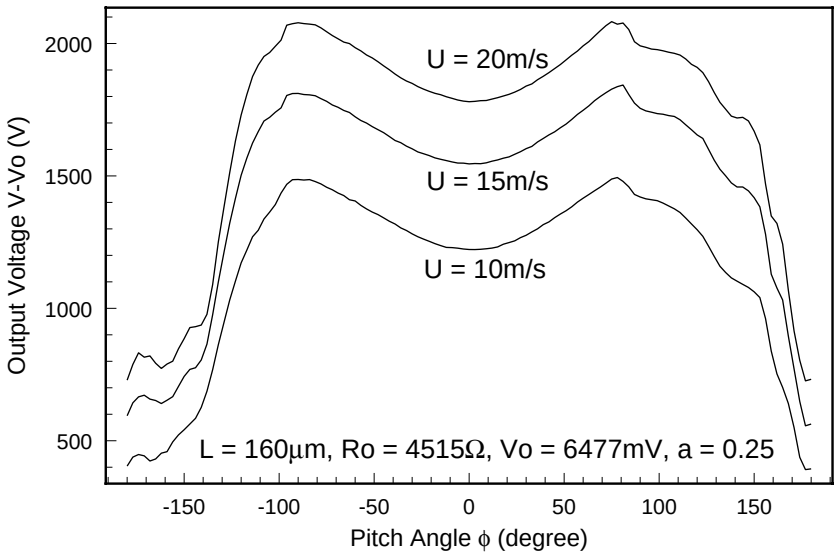

Figure 2.24 Pitch angular dependency of the 160 μm long hot wire (also used in Figure 2.22) in CT mode.

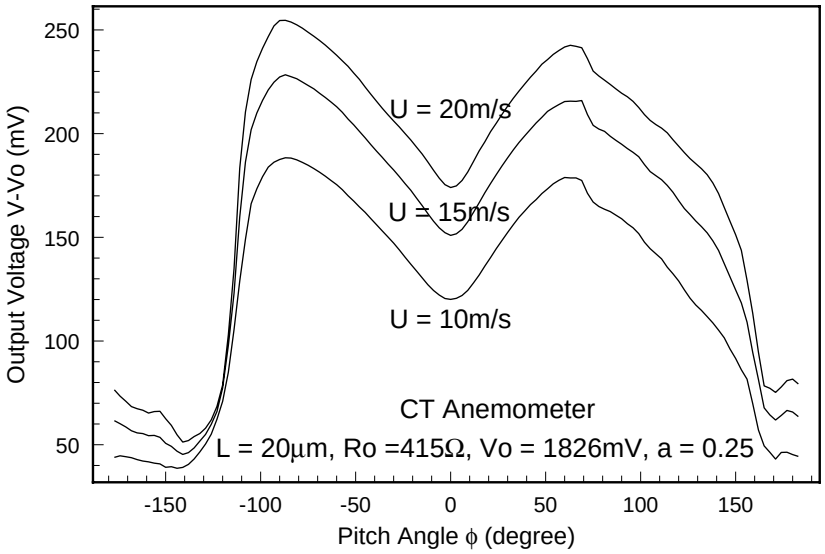

Figure 2.25 Pitch angular dependency of a 20 µm long hot wire (also used in Figure 2.23) in CT mode.

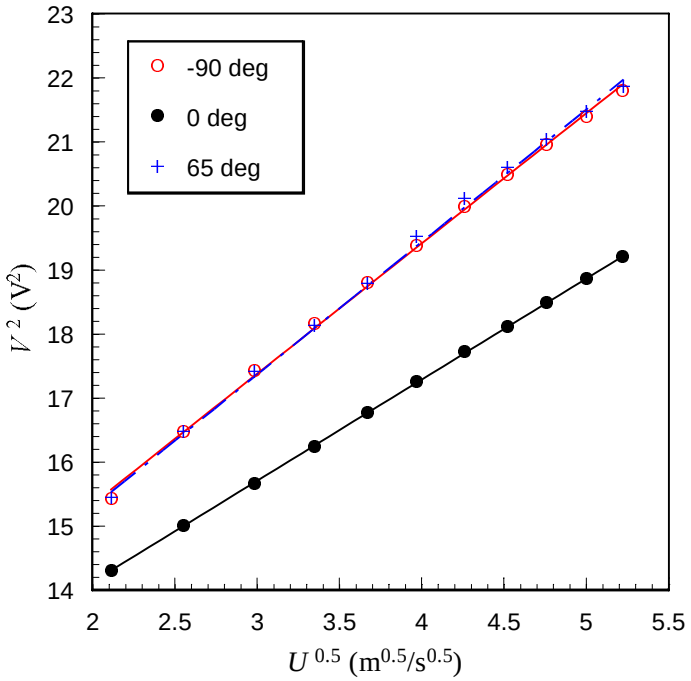

Figure 2.26 Steady-state characteristics of an 80 µm long hot wire (also used in Figs. 2.9 and 2.10) in CT mode at different pitch angles.

Finally, Figure 2.26 shows the output characteristics of the same 80 µm long hot wire

used in steady-state characterization but at three different pitch angles in CT mode. It is obvious that the V^2 vs. $U^{0.5}$ curve deviate from the linear fits at ϕ = -90^o and 65^o. As a matter of fact, the exponent *n* found from the best fitting is about 0.44 at ϕ = -90^o and 65^o. We speculate that this is also because of the trapezoidal wire cross section [18].

2.6 Discussion

2.6.1 Comparison with Conventional Hot Wires

Table 2.1 Comparison between conventional and micromachined hot wires.

Parameters	Conventional Hot Wire	Micromachined Hot Wire
fabrication	hand assembly	micromachining (mass producible)
material	Pt, W, Pt-Ir	polysilicon
TCR (%/^{o}C)	0.08 - 0.45	0.15
resistivity (Ω·cm)	5.5-31x10^{-6}	10^{-3}
density (g/cm^3)	20	2.3
thermal conductivity (W/cm·^{o}C)	0.18-2.0	0.34
specific heat (J/g·^{o}C)	0.13	0.7
length	1 mm	10-160 μm
diameter (μm)	5	1 μm (width) 0.5 μm (thickness)
power (mW)	4-8	2-4
current (mA)	10-15	1-2
sensitivity (CC) at 27 m/s (mV)	80	50-400
sensitivity (CT) at 27 m/s (mV)	300	100-2000
time constant (CC) (μs)	500	5-50
bandwidth (CT) (MHz)	0.15	0.5-1.4
directional sensitivity (yaw)	good	good (long wires) bad (short wires)
directional sensitivity (pitch)	small	large

Table 2.1 gives the overall comparison between a typical conventional hot wire and our micromachined hot wires. The performances are based on the measurement results at over-heat ratio of 0.25.

2.6.2 Small Aspect-Ratio Wires

Conventional hot wires with short length or small aspect ratios are normally not used in flow velocity measurement because they are difficult to make, their resistance and sensitivities are too low, and serious conduction losses to the supports cause dynamic effects that are difficult to measure experimentally [4]. However, for micromachined hot wires, the first two problems no longer exist. The sensitivity is low for short wires compared to the long wires in its own kind, but is more than enough to be detected. The last problem is still questionable, even though the calculated frequency response to velocity signal is shown to be flat all the way to its cutoff frequency. More analysis and tests need to be done. If this problem is not serious, the short micromachined hot wires would be useful in some special areas where fast response and high spatial resolution are desired.

2.6.3 Center-Lightly Doped Hot Wires

It is well known that lightly doped polysilicon has very high resistivity and large negative TCR (up to -1%/^{o}C). Therefore, a uniformly and lightly doped polysilicon hot wire could have an unprecedented high sensitivity. However, its resistance would be so high that it would require an extremely high voltage to operate. To avoid this problem, we have designed a center-lightly doped polysilicon hot wire which is geometrically the same as Figure 2.2, but the 2 μm center part of the wire is lightly doped. The overall dc resistance of the wire at the operating point is less than 10 kΩ. It has been confirmed that this type of hot wire indeed has a higher sensitivity than the uniformly and heavily doped hot wires. In addition, they have a smaller time constant [22]. However, these hot wires have serious stability problems due to the resistance drift caused by the dopant diffusion

from the heavily doped sides to the lightly doped middle.

2.6.4 Mechanical Rigidity

The support shanks of our hot wires are only 0.5 μm thick but are about 20 μm wide. They can not stand in high speed flows that are not in parallel with them. However, the geometry and structure is by no means the optimum for the support shanks of micromachined hot wires, and a lot of improvements can be made. For example, we can simply increase the thickness of the polysilicon to a few microns for the support shanks while keeping the thickness of the polysilicon wire at one half micron.

2.6.5 Bending of Support Shanks

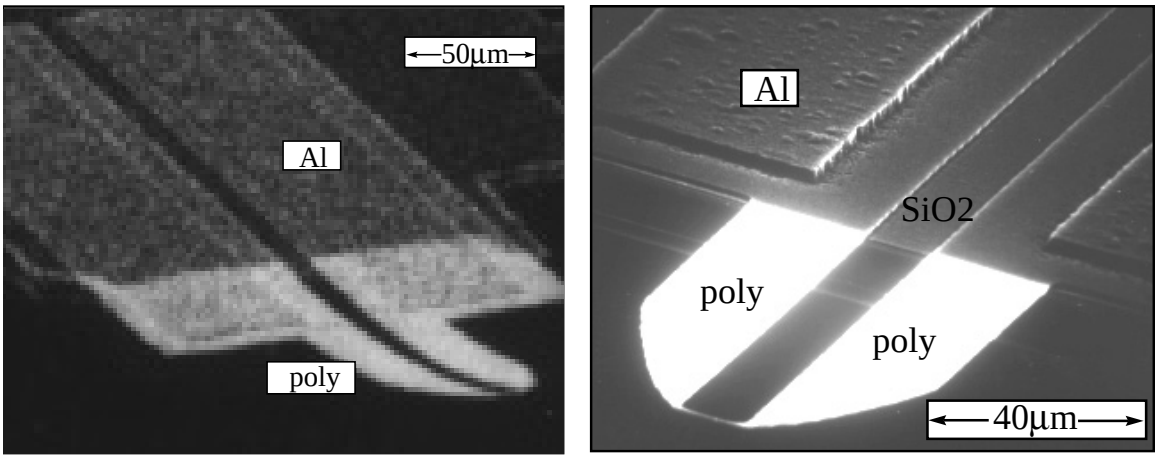

(a) (b)

Figure 2.27 SEM pictures of hot wires made from (a) polysilicon deposited at 620^{o}C; (b) crystallized amorphous silicon deposited at 560^{o}C.

As previously mentioned in the design section, we found that the stress distribution along the depth of the polysilicon deposited at 620^{o}C and annealed at 1100^{o}C is not uniform. Sometimes, the tips of all the anemometer probes in a wafer made from this type of polysilicon bend up about 50 μm, as shown in Figure 2.27(a). However, this

phenomenon is never observed in anemometers made from the polysilicon deposited at 560^{o}C and annealed at 1100^{o}C, as shown in Figure 2.27(b). The reason might be that the structure of as-deposited and as-implanted amorphous silicon films are uniform along the depth. During annealing, the grain growth is uniform, so the stress distribution is uniform too.

2.6.6 Temporal Drift

It has been observed that the resistance of hot wires increases slowly during the operation. Figure 2.28 shows the temporal drift of a 80 μm long heavily doped probe. Several factors contribute to the drift. First, the polysilicon is not protected and could be oxidized during high temperature operation. This can be avoided by a conformal anti-oxidation layer coating over the free standing polysilicon structures. This would only increase the time constant a little. Second, since dopants in polysilicon have high diffusion coefficients, the temperature non-uniformity and the electric field across the wire at the operating temperature of a few hundred degrees may cause the slow diffusion of dopants. Amemiya et al. [23] found that the resistivity of heavily doped polysilicon decreases under high current density. This contradicts our observation. Further studies need to be done on the mechanism of this drift.

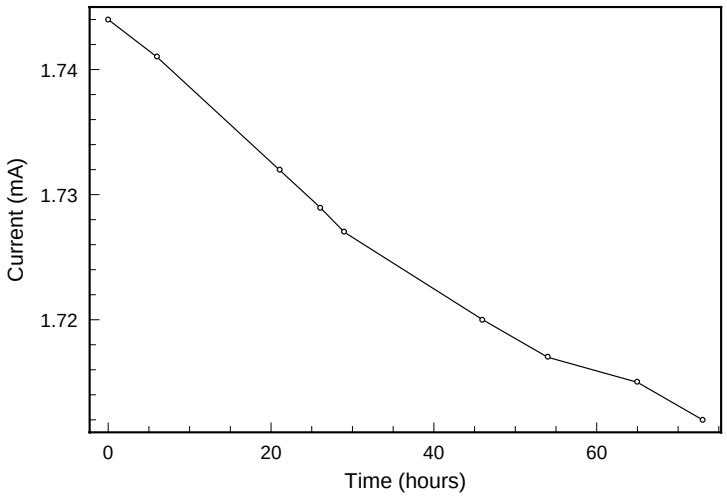

Figure 2.28 The temporal drift of a 80 μm long hot wire at V = 2.5 V and a_R = 0.35.

2.7 Summary

A new type of micromachined hot-wire anemometer has been developed. Extensive characterization of their steady-state characteristics, frequency responses and directional dependencies has been carried out. These hot wires, if properly designed, can be practical. They can significantly out-perform conventional hot wires in some aspects such as spatial resolution, sensitivity and frequency response.

Bibliography

[1] L. V. King, "On the Convection of Heat from Small Cylinders in a Stream of Fluid: Determination of the Convection Constants of Small Platinum Wires, with Application to Hot-Wire Anemometry," *Proc. R. Soc. London*, Vol. 90, pp. 563-570, 1914.

[2] R. F. Blackwelder, "Hot-Wire and Hot-Film Anemometers," *Methods of Experimental Physics: Fluid Dynamics*, Vol.18, Part A, Academic Press, pp. 259-314, 1981.

[3] A. E. Perry, *Hot-Wire Anemometry*, Clarendon Press, 1982.

[4] L. M. Fingerson and P. Freymuth, "Thermal Anemometers," *Fluid Mechanics Measurements*, J. Goodstein, ed., Hemisphere Publishing Corp., pp. 99-154, 1983.

[5] H. H. Bruun, *Hot-Wire Anemometry: Principles and Signal Analysis*, Oxford University Press, 1995.

[6] W. R. Runyan and K. E. Bean, Semiconductor Integrated Circuit Processing Technology, Addison-Wesley, 1990.

[7] K. E. Petersen, "Silicon as a Mechanical Material," *Proc. IEEE*, Vol. 70, pp. 420-457, 1982.

[8] G. Kaminsky, "Micromachining of Silicon Mechanical Structures," *J. Vac. Sci. Technol. B*, Vol. 3, pp. 1015-1024, 1985.

[9] L. Lofdahl, G. Stemme, and B. Johansson, "Silicon Based Flow Sensors Used for Mean Velocity and Turbulent Measurements," *Experiments in Fluids*, Vol. 12, pp. 270-276, 1992.

[10] H. Rahnamai and J. N. Zemel, "Pyroelectric Anemometers: Preparation and Velocity Measurements," *Sensors and Actuators*, Vol. 2, pp. 3-16, 1981.

[11] Y. C. Tai and R. S. Muller, "Lightly Doped Polysilicon Bridge as a Flow Meter," *Sensors and Actuators*, Vol. 15, pp. 63-75, 1988.

[12] B. W. van Oudheusden and J. H. Huijsing, "Integrated Silicon Flow Direction Sensor," *Sensors and Actuators*, Vol.16, pp. 109-119, 1989.

[13] H. Seidel, "The Mechanism of Anisotropic Silicon Etching and its Relevance for Micromachining," *Digest IEEE Int. Conf. On Solid-State Sensors and Actuators* (*Tansducers'87*), pp. 120-125, 1987.

[14] R. T. Howe, "Surface Micromachining for Microsensors and Microactuators," *J. Vac. Sci. Technol. B*, Vol. 6, pp. 1809-1813, 1988.

[15] L. S. Fan, Y. C. Tai, and R. S. Muller, "Integrated Movable Micromechanical Structures for Sensors and Actuators," *IEEE Trans. Electron Devices*, Vol. 35, pp. 724-730, 1988.

[16] G. Harbeke, L. Krausbauer, E. F. Steigmeier, A. E. Widmer, H. F. Kappert, and G. Neugebauer, "Growth and Physical Properties of LPCVD Polycrystalline Silicon Films," *J. Electrochem. Soc*., Vol.131(3), pp. 675-682, 1984.

[17] F. Jiang, Y. C. Tai, C. M. Ho, K. Rainer, and M. Garstenauer, "Theoretical and Experimental Studies of Micromachined Hot-Wire Anemometer," *Digest IEEE Int. Electron Devices Meeting (IEDM)*, San Francisco, pp. 139-142, 1994.

[18] M. Jakob, *Heat Transfer*, Vol. 1, John & Wiley, New York, pp. 559-564, 1949.

[19] C. H. Mastrangelo, *Thermal Applications of Microbridges*, Ph. D. Thesis, University of California, Berkeley, 1990.

[20] Y. C. Tai, C. H. Mastrangelo, and R. S. Muller, "Thermal Conductivity of LPCVD Polycrystalline Silicon," *J. Appl. Physics*, Vol. 63, pp. 1442-1447, 1988.

[21] C. G. Lomas, *Fundamentals of Hot Wire Anemometry*, Cambridge University, 1986.

[22] F. Jiang, Y. C. Tai, C. M. Ho, and W. J. Li, "A Micromachined Polysilicon Hot-Wire Anemometer," *Digest Solid-State Sensors & Actuator Workshop*, Hilton Head, SC, pp. 264-267, 1994.

[23] Y. Amemiya, T. Ono, and K. Kato, "Electrical Trimming of Heavily Doped Polycrystalline Silicon Resistors," *IEEE Trans. Electron Devices*, Vol. ED-26, No. 11, pp. 1738-1742, 1979.